Synthesis of Multifunctional Single Wall Carbon Nanotube - Amorphous Diamond Thin Film Composites

David B. Geohegan[a], C. Henrik Schittenhelm[b], Alex A. Puretzky[c], Michael J. Lance[a], Gerald E. Jellison[a], Phillip F. Britt[a]
[a]Oak Ridge National Laboratory, Oak Ridge, TN 37831
[b]Robert Bosch GmbH, Corporate Research and Development, Stuttgart, Germany
[c]Dept. of Materials Science and Engineering, University of Tennessee

ABSTRACT

The first thin-film single-wall carbon nanotube (SWNT) composites synthesized by pulsed laser deposition (PLD) are reported. Ultrahard, transparent, pure-carbon, electrically-insulating, amorphous diamond thin films were deposited by PLD as scratch-resistant, encapsulating matrices for disperse, electrically conductive mats of SWNT bundles. In situ resistance measurements of the mats during PLD, as well as ex situ Raman spectroscopy, I-V measurements, spectroscopic ellipsometry, and field emission scanning electron microscopy, are used to understand the interaction between the SWNT and the highly energetic (~ 100 eV) carbon species responsible for the formation of the amorphous diamond thin film. The results indicate that a large fraction of SWNT within the bundles survive the energetic bombardment from the PLD plume, preserving the metallic behavior of the interconnected nanotube mat, although with higher resistance. Amorphous diamond film thicknesses of only 50 nm protect the SWNT against wear, providing scratch hardness up to 25 GPa in an optically transmissive, all-carbon thin film composite.

Keywords: carbon nanotubes, laser plasmas, spectroscopy, in situ diagnostics, nanoparticles, hydrodynamics

1. INTRODUCTION

Single wall carbon nanotubes (SWNTs) exhibit exceptional mechanical,[1-3] electronic,[4] thermal, and optical properties[5] which are envisioned for new generations of strong, lightweight, multifunctional composites. SWNT are currently being explored in bulk polymer and metal-matrix composites with key difficulties encountered in dispersing the nanotubes and forming strong bonds to the matrix material.[6-8] In this report, pulsed laser deposition (PLD, a versatile method for thin-film synthesis) is explored for the first time to encapsulate SWNT in a thin film composite. Purified SWNT were sprayed from solution and dried to form disperse, electrically-conductive interconnected mats on SiO_2 and Si substrates. Interconnected mats of SWNT exhibit pseudometallic behavior for a wide range of temperatures and applied fields[11], and might be used to lend electrical conductivity, electrostatic protection, and thermal dissipation paths in matrices of polymers and other materi-

Photon Processing in Microelectronics and Photonics II, A. Piqué, K. Sugioka, P. R. Herman, J. Fieret, F. G. Bachmann, J. J. Dubowski, W. Hoving, K. Washio, D. B. Geohegan, F. Träger, K. Murakami, Editors, Proceedings of SPIE Vol. 4977 (2003) © 2003 SPIE · 0277-786X/03/$15.00

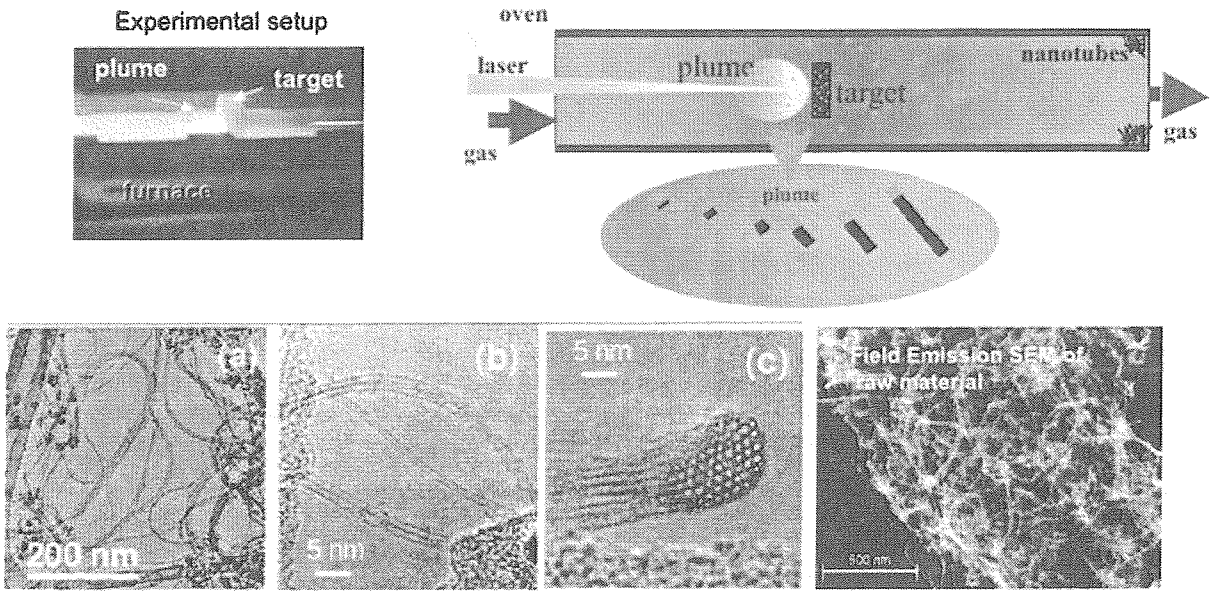

Fig. 1. Laser ablation of a carbon target (with 1 at.% each of Ni and Co as catalysts) in a tube furnace at 1150 C with 500 Torr Argon (flowing 100 sccm) was used to synthesis single wall carbon nanotubes (SWNT). The nanotubes form in the plume during its traversal through the furnace, and are collected outside the hot zone of the furnace.

als.

2. EXPERIMENTAL RESULTS

In this study, a matrix of amorphous diamond (tetrahedrally-coordinated amorphous carbon (*ta*-C))[9,10] was deposited by PLD to encapsulate the SWNT mats, forming a pure-carbon nanocomposite. The amorphous diamond film is intended to

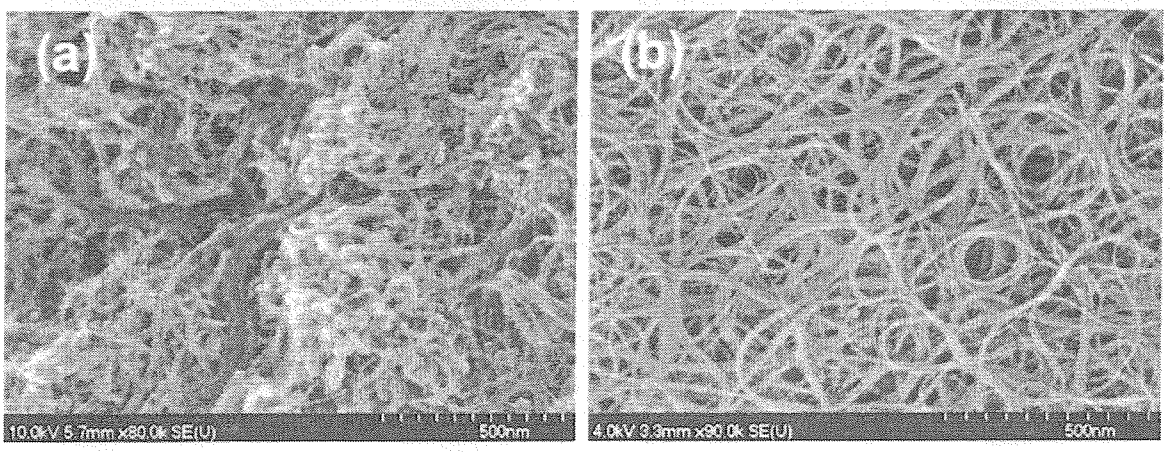

Fig. 2. Purification of single-wall carbon nanotubes utilized a combination of acid etching with 3M HNO_3 in H_2O, followed by rinsing, drying, and subsequent oxidation for ~ 30 minutes at 500°C in air. The acid etch dissolves the metal particles left in the raw nanotube material, whereas the subsequent oxidation burns away the amorphous carbon without significantly damaging the SWNT. (a) Raw SWNT Material. (b) Purified SWNT "Buckypaper"

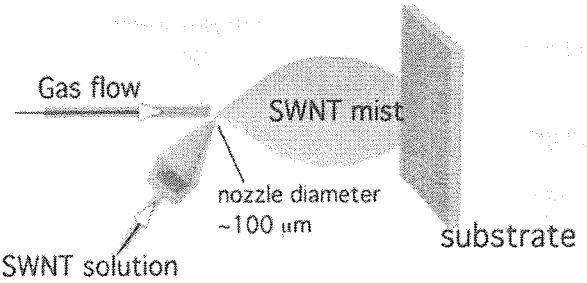

Fig. 3. Automated spraying of purified SWNT suspended in dicholoroethane (DCE) was performed with a commercial airbrush at various pressures onto Si and SiO_2 substrates. Dispersed SWNT mats of varying areal bundle densities and diameters could be achieved by applying different solvent concentrations and spraying strategies, resulting in interconnected nanotube mats with different resistivities.

provide a hard, scratch-resistant, transparent, and electrically insulating coating for the electrically-conductive, disperse mats of SWNTs and serve as an abrasion-resistant barrier to ambient gases and liquids, which have been observed to strongly influence the electronic properties of SWNT.[12,13]

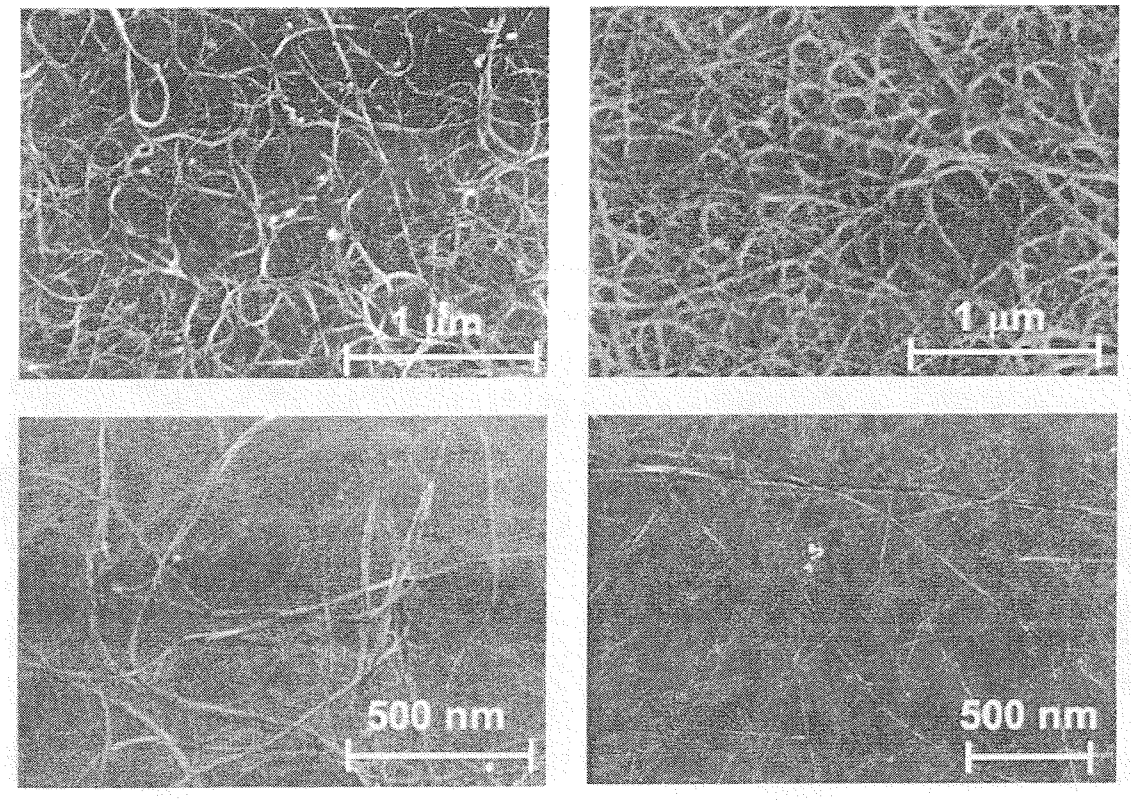

Fig. 4. SEM images of SWNT bundles on Si substrates deposited by solution spraying. By adjusting the spray duration, solvent concentration, nozzle pressure and spraying strategy the diameter of the bundles and the areal density of the interconnected SWNT mats can be controlled, thereby adjusting physical properties of the coating (e.g. resistivity). I-V curves of the interconnected mats showed metallic behavior, and resistances could be varied over several orders of magnitude.

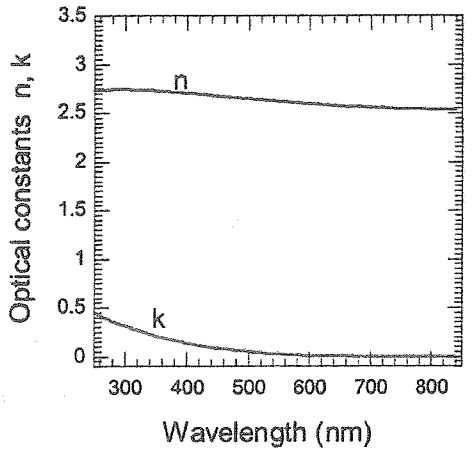

Fig. 5. Optical properties of the ta-C/SWNT/Si composite films. Spectroscopic ellipso-metry measurements of the *ta*-C films indicate an E_g = 1.84 eV. This corresponds to an sp^3 content of ~ 70% and ~ 40 GPa hardness.

As shown in Figure 1, the SWNTs were synthesized by laser vaporization[14] of a Dylon® target (with 1 at.% of Ni and Co each as catalysts) in a tube furnace at 1150 C and 500 Torr Argon (flowing at 200 sccm). As shown in Figure 2, the SWNT were purified from amorphous carbon and metallic catalyst particles by a procedure which involves etching for 16 hours in 3M HNO_3 in H_2O, followed by rinsing, drying, and subsequent oxidation for up to 90 minutes at ~500 C.[15,16] Energy dispersive X-ray analysis and thermogravimetric analysis indicate that less than 0.5 weight % of residual metal catalyst particles remain in the purified SWNT.

The purified SWNT were dispersed in distilled dichlorethane (DCE) at concentrations of about 1mg/ml and spray-deposited onto Si and SiO_2 (Suprasil fused silica) substrates with a commercial airbrush apparatus (see Fig. 3). The SWNT/

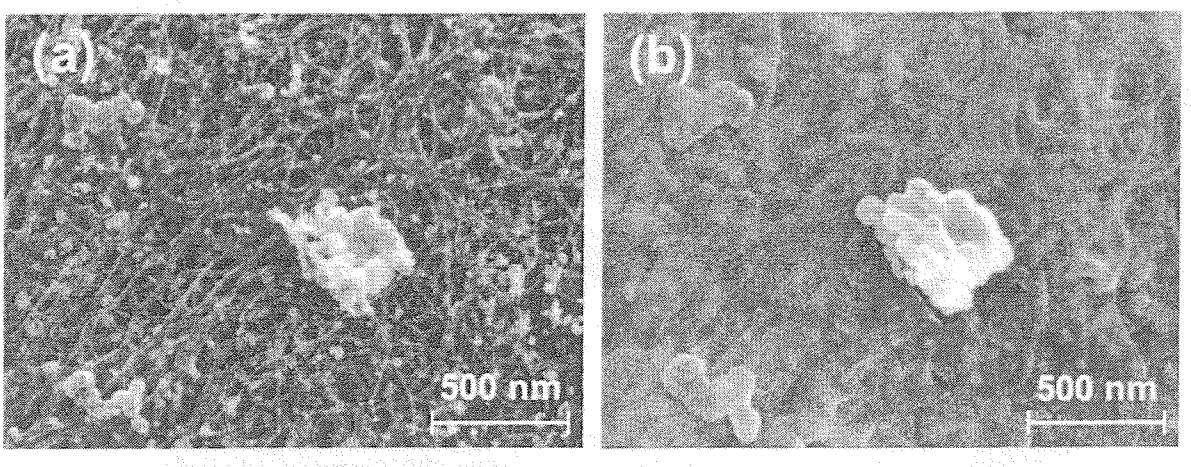

Fig. 6. FESEM imaging of a SWNT mat on a Si substrate before (left) and after (right) amorphous diamond thin film deposition.

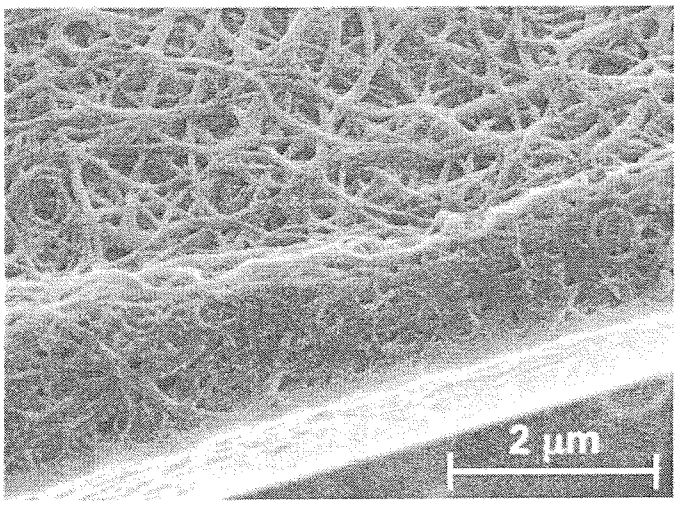

Fig. 7. FESEM image of a thick mat of SWNT bundles on a Si substrate covered with a thin film of amorphous diamond like carbon.

DCE solution was sonicated during the spraying process to inhibit SWNT aggregation while a motorized x-z stage was used to move the airbrush nozzle parallel to the substrate to obtain uniform SWNT dispersal on the substrates. By adjusting the spray duration, solvent concentration, nozzle pressure and spraying strategy the diameter of the bundles as well as the areal density of the interconnected SWNT mats could be controlled, thereby adjusting the resistance of the coating (Figure 4).

The nanotube laden substrates were then subjected to PLD conditions optimized for amorphous diamond film

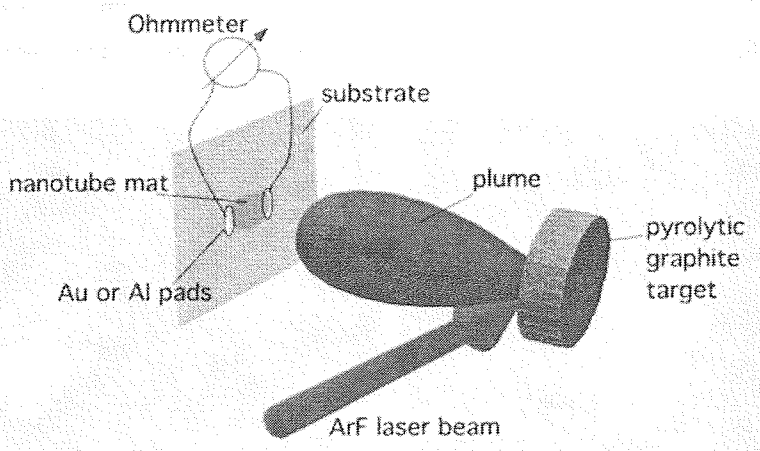

Fig. 8. Schematic of the pulsed laser deposition geometry with in situ resistivity measurements. A sprayed SWNT network was applied on an oxide-coated Si wafer with prepatterned gold or aluminum pads. The resistance of the SWNT network on the wafer was monitored via the two-point resistivity method during laser ablation of a pyrolytic graphite target in vacuum. The metal pads and electrode contacts were shielded from the plume during film deposition.

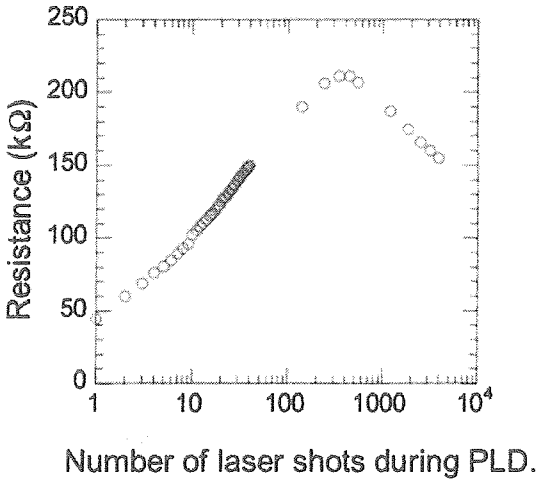

Fig. 8. Typical resistance of a SWNT mat vs. the number of laser shots during PLD of amorphous diamond coatings. The rise of the resistivity during deposition correlates with the first few nm of *ta*-C film formation, which requires the creation of an interfacial layer and reordering of the sp^2 bonds. The subsequent drop in resistivity probably occurs due to improved intertube contact resulting from the compressive stress in the film.

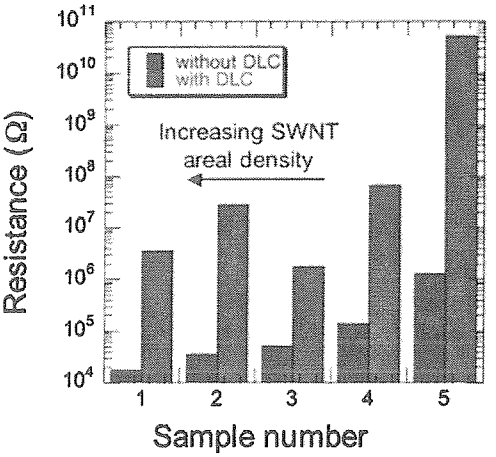

Fig. 9. Resistance before and after ta-C film deposition for thin SWNT films on Quartz substrates.

formation in vacuum.[17] An ArF-excimer laser irradiated (energy density F ~1.8 J/cm^2) a pyrolytic graphite target in vacuum (~10^{-5} Torr), generating C^+ ions with most-probable kinetic energies ranging from 80-100 eV as measured with an ion probe.[18] These fast carbon ions and neutrals, along with slower C_2 and C_3 molecules, have sufficient kinetic energy to form amorphous diamond films on Si or SiO_2 substrates. However, it was unclear whether adherent films of amorphous diamond could be formed on webs of interconnected SWNT bundles which comprise up to 40% of the areal coverage (as shown in Fig. 4). After PLD in vacuum (at d = 7 cm), of film thicknesses between 10 nm and 50 nm (at rates of about 0.1 nm/s (0.01 nm/laser shot)), adherent films were found to conformally coat the SWNT in transparent, hard thin films as shown in Figures 6 and 7.

An HP 4156A Precision Semiconductor Parameter Analyzer was first used to measure the current-voltage characteristics of interconnected SWNT mats on SiO_2 substrates. Contact to the nanotube mat was made using evaporated Al pads on the SiO_2 which were deposited before nanotube spraying. All mats exhibited metallic behavior for applied voltages between -10V and +10V, however depending upon the areal density of the nanotubes forming the mat, resistances were varied between 15 kW and 1 MW over 1 cm distances. A Keithley 195 System digital multimeter monitored the resistance of the SWNT mat in situ during deposition of the *ta*-C film, while the Al pads and contact leads were shielded from the PLD plume. In each case, an initial rapid increase in the resistance was observed after each of the first 5-10 PLD pulses which was probably caused by the desorption or damage of some of the SWNTs by the impact of the energetic carbon ions and neutrals. The resistance continued to increase slowly over the first few nm of film thickness, and then stabilize or decrease with further

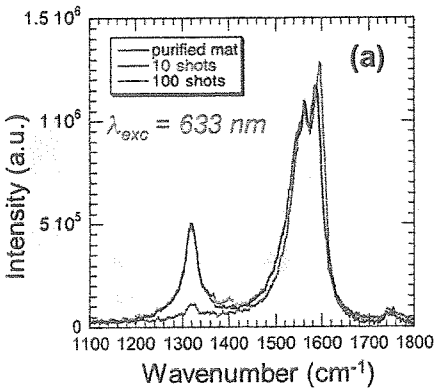

Raman signals for different ta-C film thicknesses on a pure SWNT mat

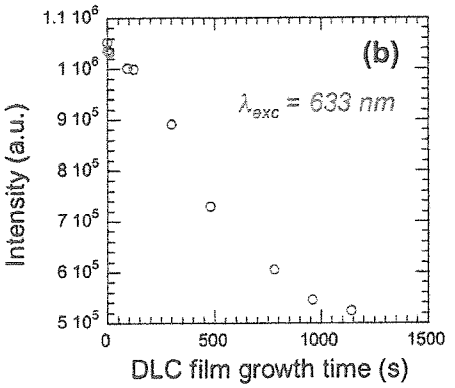

1562 cm^{-1} SWNT Raman TM band intensity for different ta-C film thicknesses

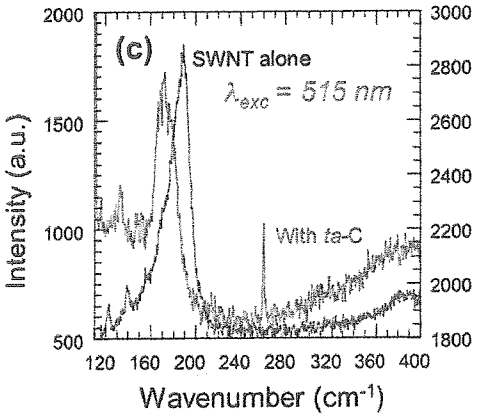

Raman spectra in the SWNT breathing mode region before and after ta-C deposition.

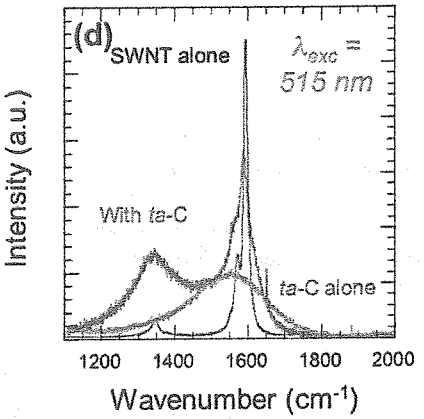

Raman spectra in the SWNT tangential mode region before and after ta-C deposition.

Fig. 10. Resonant Raman spectra from the SWNT before and after *ta*-C film deposition show that the characteristic SWNT tangential and breathing modes are still present, but decreased in magnitude, indicating that a large fraction of SWNT survive the energetic deposition process. The presence of amorphous carbon, most likely at the SWNT/ *ta*-C interface, is indicated by the broad bands at 1350 cm^{-1} and 1580 cm^{-1}. Raman spectroscopy of the SWNT mat before and and after the deposition shows anincreasing D-band probably due to damage of the tubes by high energy C ions.

deposition. I-V curves were then remeasured ex-situ, and metallic behavior was again observed for the coated mats, however the resistance ranged from a factor of 3 to a factor of 10^4 higher after *ta*-C film deposition (resistances from 45 kW to 10^4 MW). By comparison, resistances for pure *ta*-C films were 6×10^5 MΩ over a distance of 1 cm. In general, mats consisting of high areal densities and thicker bundles of SWNT resulted in smaller increases in resistance after deposition. In each case, the metallic behavior of the SWNT mat was preserved.

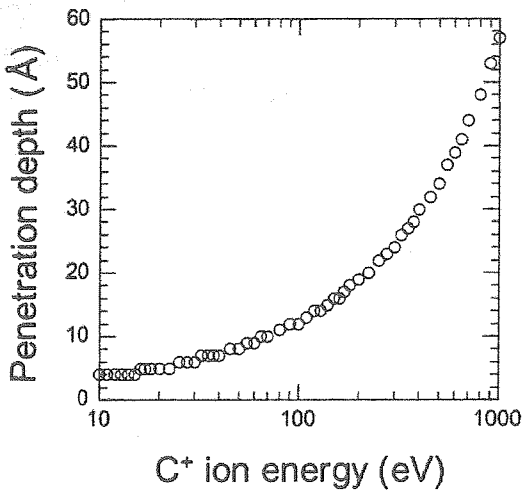

Fig. 11. Predicted penetration depth of carbon ions into SWNT bundles (density assumed 1.33 g/cm3).

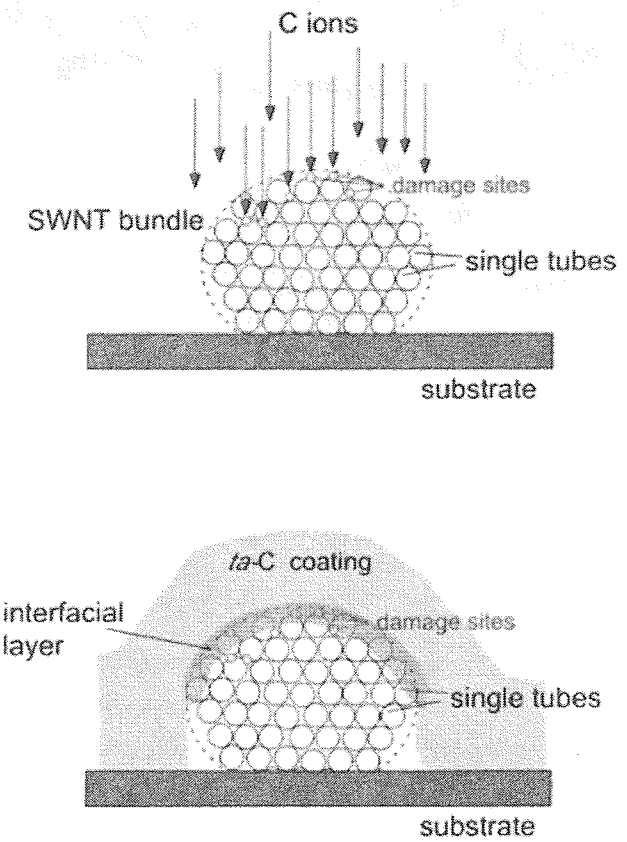

Fig. 12. Physical model of the deposition process. Incident C^+ ions with kinetic energies around 100 eV cause damage to the upper layers of tubes in the SWNT bundles resulting in the increase of the Raman D-band. The penetration depth of these ions is around 1 nm and, therefore, defects should be located on the upper layers of a SWNT bundle. During the deposition of this layer, the resistance of the interconnected nanotube mat increases. The smaller the bundle diameter, the higher the fraction of damaged SWNTs which should be expected. Thin mats of SWNT with the smallest bundle diameters show the strongest increase in the resistance of the SWNT mat after *ta*-C deposition.

Spectroscopic ellipsometry measurements of a pure *ta*-C film and a representative *ta*-C/SWNT composite film (on Si substrates) are shown in Fig. 5, which assumes a Tauc-Lorentz model with variable surface void fraction to account for surface roughness.[19] First, the pure *ta*-C film is of high quality, with a high ($n > 2.5$) index of refraction and low absorption across the visible, corresponding to a bandgap of 1.84 eV and a hardness of ~ 40 GPa.[18] The effective medium comprised of *ta*-C with embedded SWNT exhibits a slightly lower refractive index and the expected higher absorptivity. However, good optical access to the embedded nanotubes is achieved since $k = 0.19$ at 500nm (close to 514 nm used for Raman probing) for the composite film, corresponding to an absorption coefficient of 48000 cm^{-1} and an 80% transmission through the 50 nm-thick film.

Resonant Raman spectra from the SWNT mats before and after *ta*-C film deposition are shown in Fig. 10. Although decreased in magnitude, the characteristic tangential (TM) and breathing (BM) modes are preserved indicating that a large fraction of SWNT survive the energetic deposition process. The Raman spectrum of the *ta*-C/SWNT composite in Figure 10 displays a combination of the SWNT TM and a broad "G-band" from the amorphous diamond coating. Depending on the areal density of the SWNTs before *ta*-C film deposition the TM mode feature in the composite film ranges from barely observable to very pronounced (as in Fig. 10). A slight red shift of both the Raman BM and TM signals from the SWNTs was

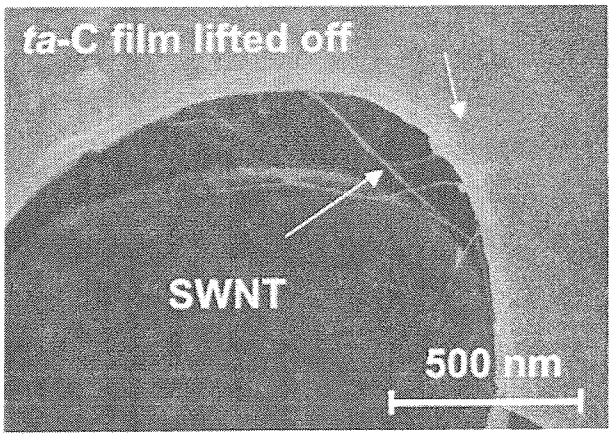

Fig. 13 SEM image of a crack in the *ta-C* coating revealing apparently intact SWNT bundles underneath the film. Raman spectroscopy confirms that the SWNTs are intact underneath the *ta-C* film and resistance measurements confirm that their electrical transport properties are preserved.

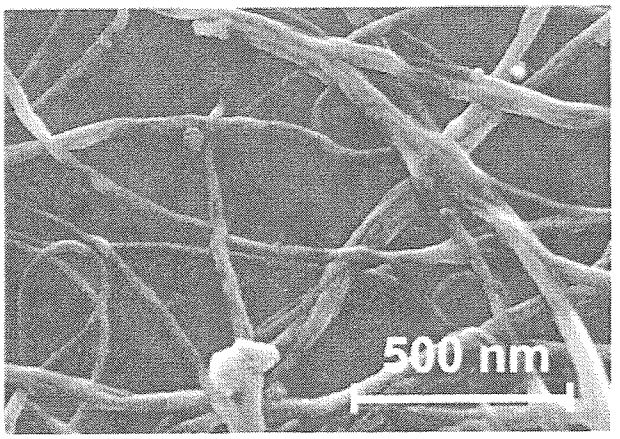

Fig. 14. SEM image of the resistive nanotube network of SWNT covered with a protective layer of *ta-C* (amorphous diamond). The *ta-C* coating forms an optically transparent, hard, scratch-resistant and chemically-protective coating to preserve the electronic properties of the interconnected nanotube network.

observed and is counterintuitive to the expected compressive strain of the SWNT from the *ta*-C film.

Figure 12 summarizes a model for *ta*-C /SWNT film formation consistent with the experimental results. High energy C^+ ions and neutrals during PLD introduce defects in the upper layers of the SWNT bundles, affecting interconnections between bundles in the mats, resulting in the increased mat resistance. Kinetic model simulations with a Monte Carlo TRIM code estimated a ~ 1-nm penetration depth for 100 eV C^+ ions into SWNT bundles (estimated 1.33 g/cm^3 density) as shown in Figure 11. Hence, defects should be located within a few upper layers of a SWNT bundle. After the first few nm of amorphous diamond film formation, which requires the creation of an interfacial layer and reordering of the sp^2 bonds, the SWNT bundles should be protected from further damage. Thinner bundles thereby experience a higher defect ratio than thicker bundles. High areal densities, where parts of some bundles are shielded by others on top of them, lead to a lower ratio of damaged nanotubes.

The synthesized composites were tested for wear resistance and scratch hardness. As schematically shown in Figure 15, a steel test ball (2g load, approximately 1.2×10^{-3} mm^2 contact area, load ~15 GPa) was moved across the SWNT mats on SiO_2 with and without protective amorphous diamond coatings while the resistance of the mats was monitored in-situ. As shown in Figure 16, the uncoated SWNT mats show a drastic increase in resistance after even one wear cycle. The resistance slowly saturates for more wear resistance lines (20 lines and more). Scanning electron microscopy (Figure 17) of the unprotected mat after wear testing showed that the thicker bundles were preferentially removed during the first few wear cycles, followed by the subsequent removal of thinner bundles. At the point of saturating resistance, only very thin bundles and single tubes were left on the surface to maintain conductivity of the mat. On the other hand, the *ta*-C/SWNT composite films showed high wear resistance compared to the uncoated mats. No increase in the resistance could be observed for up to 30 wear cycles. Scratch hardnesses of up to 25 Gpa were measured for the *ta*-C/SWNT composite films on Si using a diamond scratch tester with a spherical diamond tip of 75 mm and loads between 10 g and 100g.

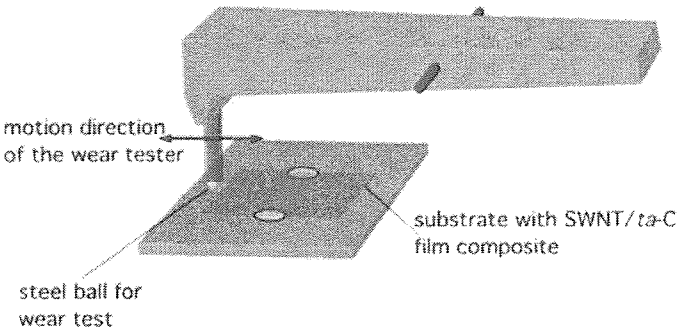

Fig. 15. The synthesized SNWT/*ta*-C film composites were tested for wear resistance. Schematic of the test procedure. A steel test ball (2g, 0.06 mm^2 contact area, ~100 GPa) was moved across the SWNT mats with and without protective *ta*-C coatings while the resistance of the mats was monitored.

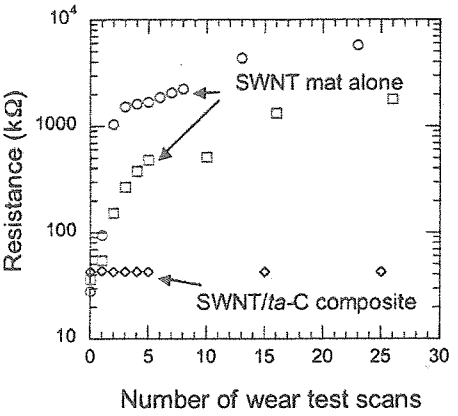

Fig. 16. The SWNT mat coated with a *ta*-C film shows high wear resistance compared to SWNT mats without the coating.

The results indicate that pulsed laser deposition (PLD) can be used to form ultrahard, transparent, pure-carbon amorphous diamond thin films as matrices to encapsulate and provide scratch-resistance for electrically conductive, disperse mats of SWNT. Moreover, PLD most often is performed in background gases where incident kinetic energies are far lower (< 1 eV). PLD therefore appears to provide a versatile method to incorporate SWNT or nanowires into thin films for the exploration of multifunctional thin film composites.

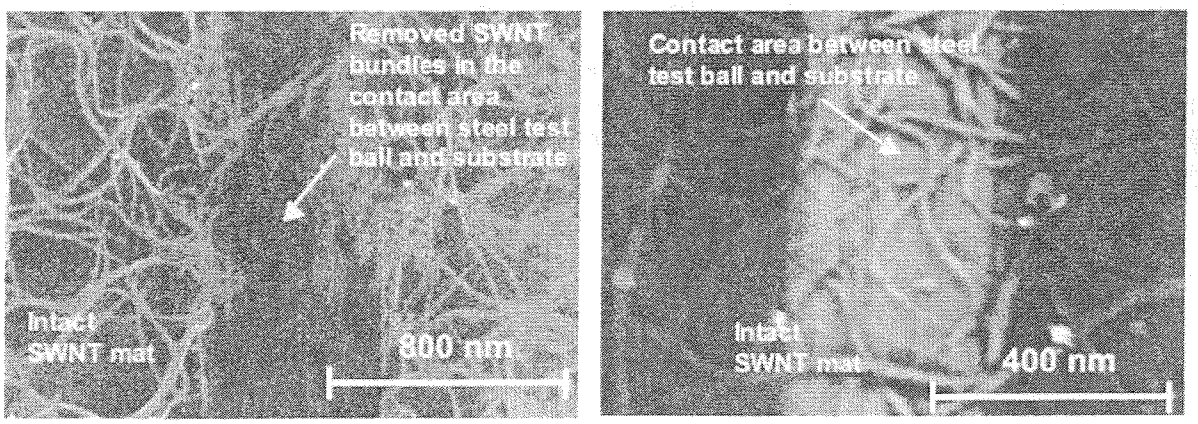

Fig. 17. FESEM images of *ta*-C coated and uncoated SWNT mats after wear-testing show that the *ta*-C coating protects the SWNT against abrasion. Without the coating, (left) nanotubes are abraded within a few wear cycles. With the coating, (right) a wear mark is evident due to the different charging of the film in the SEM, however the intact nanotube network is visible in the image under the wear track.

3. CONCLUSIONS

In summary, a new all-carbon multifunctional nanocomposite was synthesized using laser-vaporization produced single-wall carbon nanotubes in conjunction with pulsed laser deposition of tetragonally-coordinated amorphous carbon (*ta-C*, amorphous diamond). First, a spray-deposition technique was developed to form coatings of disperse mats of purified single-wall carbon nanotube (SWNT) bundles on various substrates with varying resistance and metallic I-V behavior. Second, pulsed laser deposition (PLD) was utilized for the first time to encapsulate the interconnected SWNT into a thin-film composite with enhanced functionality.

The thin coatings of tetragonally-coordinated amorphous carbon (*ta*-C) were created by pulsed laser (193-nm) ablation of a pyrolytic graphite target in vacuum. High-energy (~100 eV) carbon ions were generated and were responsible for the high sp^3 content of the deposited films, as verified by spectroscopic ellipsometry. Simulations predict that the 100-eV C^+ ions generated in the PLD process necessary to produce the *ta*-C layer should penetrate ~ 1-nm into a SWNT bundle, and preserve most of the nanotubes in the bundle. In situ resistance measurements of the SWNT mats during PLD of the *ta*-C layer indicated initial damage or desorption of the mats, followed by densification and consolidation of the composite properties.

Resonant Raman spectra from the SWNT before and after *ta*-C film deposition show that the characteristic SWNT tangential and breathing modes are basically unchanged in shape, but decreased in magnitude, indicating that a large fraction of SWNT survive the energetic deposition process given a sufficient initial thickness of the SWNT layers. The presence of amorphous carbon, most likely at the SWNT/*ta*-C interface, is indicated by the broad bands at 1350 cm^{-1} and 1580 cm^{-1}.

Wear testing experiments of the coated and uncoated SWNT-film indicate that amorphous diamond thin films can be used as protective matrices for multifunctional SWNT composites. These films provide a wear-resistant coating to shield the SWNT against mechanical deformation and environmental exposure. In addition, amorphous diamond films are ultrahard, optically transparent, electrically insulating and preserve the metallic behavior of the interconnected SWNT mats.

This proof-of-principle experiment demonstrates that pulsed laser deposition can be used as a technique to encapsulate and lend additional functionality to assemblies of nanomaterials. Pulsed laser deposition usually involves the impingement of atoms and ions with far lower (~ 1 eV or below) kinetic energies. The encapsulation of single walled carbon nanotubes without destruction by carbon atoms and ions using high (~ 100 eV) kinetic energies implies that a wide range of other films may be used to form novel nanocomposite materials by pulsed laser deposition.

ACKNOWLEDGMENTS

The authors gratefully acknowledge the assistance of P. H. Fleming, P. J. Blau, R.D. Ott, M. A. Guillorn, and T. E. Haynes. This work was supported in part by NASA Langley Research Center, and the Laboratory-Directed Research and Development Program at Oak Ridge National Laboratory, managed by UT-Battelle, LLC, for the U.S. Department of Energy under contract No. DE-AC05-00OR22725.

REFERENCES

1. L. Vaccarini, C. Goze, L. Henrard, E. Hernandez, P. Bernier, and A. Rubio, *Carbon* **38**, 1681 (2000).
2. R. S. Ruoff and D. C. Lorents, *Carbon* **33**, 925 (1995).
3. Z. L. Wang, P. Poncharal, and W. A. de Heer, *J. Phys. Chem. Solids* **61**, 1025 (2000).
4. T. W. Tombler, C. Zhou, L. Alexseyev, J. Kong, H. Dai, L. Liu, C. S. Jayanthi, M. Tang, and S. Y. Wu, *Nature* **405**, 769 (2000).
5. N. Minami, S. Kazaoui, R. Jacquemin, H. Yamawaki, K. Aoki, H. Kataure, and Y. Achiba, *Synthetic Metals* **116**, 405 (2001).
6. R. Andrews, D. Jacques, A. M. Rao, T. Rantell, F. Derbyshire, Y. Chen, J. Chen, and R. C. Haddon, *Appl. Phys. Lett.* **75**, 1329 (1999).
7. R. Haggenmueller, H. H. Gommans, A. G. Rinzler, J. E. Fischer, and K. I. Winey, *Chem. Phys. Lett.* **330**, 219 (2000).
8. C. Stephan, T. P. Nguyen, M. L. de la Chapelle, S. Lefrant, C. Journet, and P. Bernier, *Synthetic Metals* **108**, 139 (2000).
9. F. L. Xiong, Y. Y. Wang, V. Leppert, and R. P. H. Chang, *J. Mat. Res.* **8**, 2265 (1993).
10. T. A. Friedmann, J. P. Sullivan, J. A. Knapp, D. R. Tallant, D. M. Follstaedt, D. L. Medlin, and P. B. Mirkarimi, *Appl. Phys. Lett.* **71**, 3820 (1999).
11. M. S. Fuhrer, W. Holmes, P. L. Richards, P. Delaney, S. G. Louie, A. Zettl, *Synthetic Materials* **103**, 2529 (1999).
12. A. Zahab, L. Spina, P. Poncharal, and C. Marliere, *Phys. Rev. B* **62**, 10000 (2000).
13. S. Kazaoui, N. Minami, H. Kataura, and Y. Achiba, *Synthetic Metals* **121**, 1201 (2001).
14. A. A. Puretzky, D. B. Geohegan, X. Fan, and S. J. Pennycook, *Appl. Phys A* **70**, 153 (2000).
15. P. F. Britt, H. Schittenhelm, D. B. Geohegan, A. A. Puretzky, to be published.
16. A. C. Dillon, T. Gennett, K. M. Jones, J. L. Alleman, P. A. Parilla, and M. J. Heben, *Advanced Materials* **11**, 1354 (1999).
17. A. A. Puretzky, D. B. Geohegan, G. E. Jellison, and M. M. McGibbon *Appl. Surf. Sci.* **96-8**, 859 (1996).
18. V. I. Merkulov, D. H. Lowndes, G. E. Jellison, A. A. Puretzky, and D. B. Geohegan, *Appl. Phys. Lett.* **73**, 2591 (1998).
19. G. E. Jellison, Jr., V. I. Merkulov, A. A. Puretzky, D. B. Geohegan, G. Eres, D. H. Lowndes, J. B. Caughman, *Thin Solid Films* **377-378**, 68 (2000).
20. H. Schittenhelm, D. B. Geohegan, G. E. Jellison, A. A. Puretzky, M. J. Lance, P. F. Britt *Appl. Phys. Lett.* **81**, 2097 (2002)